Finite Element Analysis of Thermal Fatigue in Thermal Barrier Coatings (TBC)

C. Borri[1,*], A. Lavacchi[1], A. Fossati[1], I. Perissi[1] and U. Bardi[1]
[1]Universita` degli studi di Firenze, Dipartimento di Chimica, Via della Lastruccia 3, 50019 Sesto Fiorentino (FI)
*Corresponding author: Via della Lastruccia 3, 50019 Sesto Fiorentino (FI), borricla@libero.it

Abstract:
A Finite element model of plasma sprayed TBC's was developed to estimate the stress induced by thermal cycling experiments. A heat transfer analysis was performed to evaluate the temperature distribution on the specimen during the cooling under an impinging air jet; temperature measurements performed with an infrared pyrometer on the cooled samples show good agreement with the evaluated data. These results were then integrated in a structural mechanic model as thermal load. The COMSOL Multiphysics® Thermal-Structural interaction model allowed to determine the dependence of the stress on the temperature fields.

Keywords: FEM, Comsol Multiphysics®, Termal Barrier Coatings

1. Nomenclature

Nomenclature (units)	
d (m)	Diameter of the nozzle
g (9.81 m/s^2)	Gravity acceleration
h (W/m^2 K)	Local convective heat transfer coefficient
h_r (W/m^2 K)	Local radiation heat transfer coefficient
k (W/ m K)	Thermal conductivity of air
L (m)	Length of the heat-transfer surface
r (m)	Distance from the stagnation point (radial)
T (K)	Temperature
ΔT (K)	Temperature Difference
v (m/s)	Vertical average velocity of the jet at the nozzle exit
z (m)	Nozzle to plate distance (axial)
$Gr=L^3 \rho^2 g \beta \Delta T/ \mu^2$	Grashof Number
Nu=hL/k	Nusselt Number
Pr=α/ν	Prandtl Number
Re=ρvd/μ	Reynolds Number
Greek Symbols (units)	
α (m^2/s)	Thermal diffusivity of air
β (K^{-1})	Thermal expansion volumetric coefficient
ε	Emissivity of the heat transfer surface
σ (5.67·10^{-8} J/m^2 K^4 s)	Stefan-Boltzmann constant
μ (Pa s)	Dynamic viscosity of air
ν (m^2/s)	kinematic viscosity of air
ρ (kg/m^3)	Density of air

2. Introduction

Thermal Barrier Coatings (TBC) are widely used to protect metallic substrates from erosion and corrosion, in particular they are used in aerospace and energy applications to increase the efficiencies of gas turbines, allowing to increase the inlet turbine temperature. A typical TBC consists in an air plasma-sprayed yttria-stabilized zirconia (usually 7-8%YSZ) and a vacuum plasma-sprayed MCrAlY (where M is a metal as Co, Ni, Fe) bond coat (BC). The YSZ provides the thermal resistance, while the BC provides protection against the oxidation of the substrate. TBC have good thermal stability but in order to estimate their lifetime and durability, usually they are subjected to severe thermal cycling tests that evaluate the thermal resistance. The thermal shock resistance is defined as the capability of a material to retain its mechanical properties after being exposed to one or more thermal cycle. In thermal cycling experiments samples are warmed using a high temperature furnace and then rapidly cooled in a cold bath or with an impinging jet. Impinging air jet have received

lately a considerable attention due to their high rates of convective heat transfer coefficients, even if this high transfer rates are influenced by various parameters such as Reynolds' number of the jet, jet to plate spacing distances, radial distance from the stagnation point of the jet, nozzle diameter and more. TBC failures are often related with the thermo-mechanical stresses induced during the thermal cycling by different thermal expansion coefficients of the TC and the BC; in this cases the damage in the coating is induced close to the ceramic-metal interface and consists in the delamination or the cracking of the sample. Since the test results largely affected by the experimental set up, the use of a finite element model is useful to predict the stress distribution within the samples in order to optimize the assessment of the thermal cycling experiments. In literature there are various researches on modeling the stresses of coatings in thermal cycling experiments with finite element methods, but little of them are coupled with an heat transfer analysis, and none of them explores the effect of impinging jet cooling [1-5]; the use of an impinging air jet to increase the cooling speed of the sample in this kind of experiment could in fact introduce high thermal gradients that could accelerate the failure processes of the coating. This paper aims to use convective heat transfer coefficients found in literature to set up a finite element heat transfer analysis and to introduce the obtained results in a coupled structural mechanics model as thermal load, in order to analyze the effect of thermal gradients generated by the use of impinging jet cooling . More over the heat transfer analysis results are compared with temperature measurements performed by means of an infrared pyrometer on samples subjected to thermal fatigue cycling in order to assess the heat transfer model. In this study we didn't consider the residual stresses of the sample due to the plasma spraying process of the coating, this will be subject for further investigation.

3. Experimental

3.1 Heat Transfer Characteristic of the Jet

We consider a laminar fully developed air jet exiting with velocity v from a round nozzle of diameter d situated at a distance h from a solid surface. As the jet impinges on the surface is possible to define three different regions that show different heat transfer characteristics.
The point where the center of the jet impinges on the surface is called the stagnation point (r/d=0). Experimental measurements show that at the stagnation point, where the velocity of the jet is zero, the heat transfer coefficient is maximized, then it will decrease until it reaches a local minimum, at the end of the stagnation region (r/d=1÷1.2). After that there is the transition region (from r/d=1÷1.2 to r/d=2.5÷3) where it is possible to identify a secondary peak; this secondary peak is higher for higher Reynold's number and lower jet plate distances. After that the Nusselt number decreases monotonically in the wall jet region (r/d>2.5÷3). As shown in literature, the relative dimension of these regions are affected by the jet to plate distance and the Reynold's number of the jet.

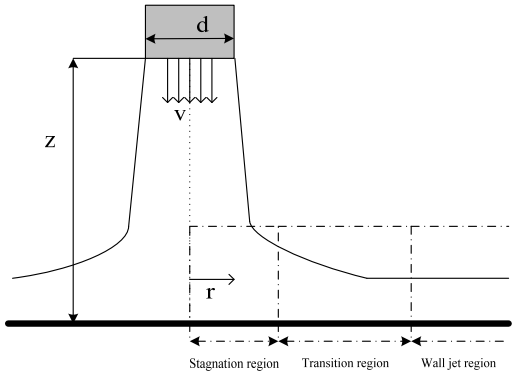

Fig.1. Different regions of an air jet impinging on a solid surface.

We used the following expression to evaluate the convective heat transfer coefficient in the stagnation region from the Nusselt number (Nu=hL/k) [6]:

$$\frac{Nu}{\mathrm{Re}^{1/2}\,\mathrm{Pr}^{1/3}} = a_1\left(\frac{z}{d}\right)^{-0.11}\left(1-\frac{\left(\frac{r}{d}\right)^{2}\left(\frac{z}{d}\right)^{-0.2}}{b_1}\right)^{1.2} \quad (1)$$

Where the constants a_1=1.5 and b_1=3.05 were evaluated from data found in literature for our experimental configuration with z/d=5.

In the transition region we used the following expression that showed to have good agreement with experimental data in literature [6]:

$$Nu = 0.198\,\mathrm{Re}^{0.6632}\left(\frac{z}{d}\right)^{-0.0826}\left(\frac{r}{d}\right)^{-0.3702} \quad (2)$$

Finally for heat transfer in the wall jet region we used this expression:

$$Nu = 0.0436(E)\,\mathrm{Re}^{0.8}\,\mathrm{Pr}^{0.333}\left(\frac{z}{d}\right)^{0.0976}\left(\frac{r}{d}\right)^{-1.0976} \quad (3)$$

Where the enhanced factor E=3.75 was evaluated from data found in literature for our experimental configuration z/d=5[6].

3.2 Numerical Formulation

Finite element analysis with Comsol Multiphysics® was performed to evaluate the thermal induced stresses during thermal cycling tests. We used the thermal-structural interaction axial symmetry stress-strain with thermal expansion, transient analysis model to assess the simulations. The experiments were carried out on a disk, so the geometry was reduced to two-dimensions due to symmetry reasons, as shown in fig. 2a. Since the MCrAlY bond coat have thermal and mechanical characteristic similar to the Inconel layer (our bond coat was a CoNiCrAlY alloy) [7,8] we assumed that the geometry of the three layers TBC could be simplified including the MCrAlY bond coat 300 μm thick in the Inconel layer. This geometry consists in two different domains: the first one is represented by the 8%-YSZ coating that is 1.5 mm thick, the second domain is made of a Inconel 718 substrate that is 6.5 mm thick, both the domains are 1.27 cm wide (radius of the sample).

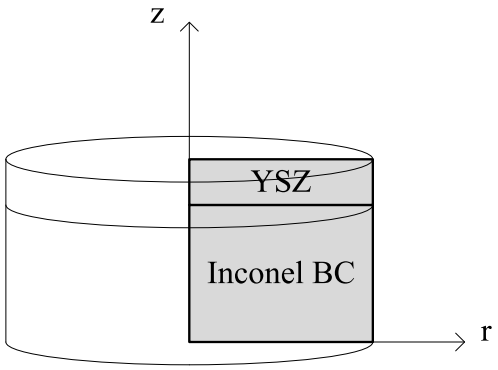

Fig. 2a. Two-dimensional symmetry reduction of the sample's geometry.

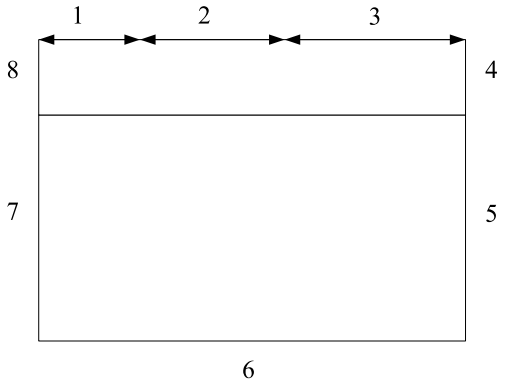

Fig. 2b. Boundaries

The temperature dependence of the physical-mechanical characteristics for the materials have been evaluated from the reference data listed in Table 1.

Properties	**8%YSZ**	**Inconel 718**
Thermal Conductivity (W/m K)	2.29 [10]	15.048 [10]
Density (kg/m^3)	6000 [10]	8510 [10]
Heat Capacity at constant pressure (J/Kg K)	600 [11]	652 [12]
Poisson's Ratio	0.23 [10]	0.3 [13]
Young's modulus (Pa)	$2.05\cdot10^{10}$ [14]	$2\cdot10^{11}$ [13]
Thermal expansion coefficient (1/K)	$1\cdot10^{-5}$ [15]	$1.15\cdot10^{-5}$ [10]

Table 1: Physical-mechanical characteristics of the materials.

We set up the following equation for the heat flux on the boundaries 1-4,6:

$$k\nabla T = h\Delta T + h_r \Delta T^4 \quad (4)$$

Where k is the thermal conductivity of the specified material, h is the convective heat transfer coefficient evaluated from the Nusselt's number values and h_r is the radiative heat transfer coefficient.
The air jet impinges the sample surface at r=0, so we use the expression (1) to evaluate the convective heat transfer coefficient in this boundary, which is the stagnation region of the jet (0<r/d<1). Boundary 2 is the transition region of the jet (0<r/d<2.5), so it has been used the expression (2) to evaluate the local convective heat transfer coefficient in this boundary. Boundary 3 is the wall jet region and the expression (3) was used for this zone. Boundary 4 is exposed to air but it is not directly impinged by the jet, so it has been used the following expression to evaluate the heat transfer coefficient for natural convection on a vertical surface [7]:

$$Nu = a\left(Gr\,\mathrm{Pr}\right)^m \quad (5)$$

Where a=1.36 and m=1/5 for L<0.91 m and $Gr \cdot Pr < 10^4$ (our experimental conditions).
A radiation heat transfer coefficient was also included in boundary conditions for the boundaries 1, 2, 3 and 4 defined as:

$$h_r = \sigma\varepsilon \quad (6)$$

Where σ is the Stefan-Boltzmann constant ($5.67 \cdot 10^{-8}$ J/m^2 K^4 s) and ε is the emissivity of the heat transfer surface (for the YSZ surface ε=0.45).
Since the sample was contained in a bracket of insulator material, we used a thermal insulation condition for boundary 5.
As for boundary 4, we used the natural convection heat transfer coefficient (5) for boundary 6, where a=0.27 and m=1/4 for a horizontal flat surface facing downward with $3 \cdot 10^5 < Gr \cdot Pr < 3 \cdot 10^{10}$, we also included as boundary condition the radiation heat transfer coefficient (6) for the Inconel surface (ε=0.6).
Finally on boundary 7 and 8 we defined axial symmetry boundary conditions.
To validate the FEM model, we performed also temperature measurements on samples with the same materials and geometry. The samples were heated in a tubular furnace with bottom charge and thermocouple temperature control, until the temperature of 1423 K for 45 minutes, then they were extracted from the furnace and cooled with an impinging air jet at room temperature (298 K) in their refractory bracket. Re of the jet was evaluated around 10000 for our working configuration, that is typical for a turbulent jet.
The thermal expansion parameters as strain temperature and strain reference temperature (1423 K) were included in the coupled stress-strain model as thermal load. With this initial conditions we assumed that the sample was completely relaxed after being heated at the working temperature, so the only thermal induced stress we obtained from the simulations were generated by the cooling of the sample.
In the structural model we used free boundary conditions in all boundaries, that allowed the deformation of the geometry as a result of the thermal contraction during cooling. We also inserted a constrain of zero displacement in both r and z directions for the origin of the axis as a condition to anchor the geometry to avoid complete displacement during simulations.

4. Results

We performed a transient analysis and since the greatest thermal gradients and stresses were supposed to be focused on the stagnation point (B) of the jet on the YSZ surface and on the interface between the YSZ layer and the Inconel substrate at the edge of the sample (point A), we chose to use smaller elements (maximum dimension of the element=$1 \cdot 10^{-5}$m) as shown in Fig. 3 in this regions; the final number of elements was 7581. Further refinement of the meshing didn't provide a quality improvement of the results, while increased sensibly the simulation time. All the simulations were carried out on a Linux workstation equipped with 4 Gb of RAM and a 3.60 GHz Intel Pentium 4 processor. The COMSOL Multyphysics® release used for the present investigation was the 3.4.

Fig.3. Meshed domains.

Fig. 4 shows temperature distribution of the cross-section of the sample, for different times (from t=0.1 s to t=300 s with time steps of 0.1 s). As we expected, the thermal gradients were generated in the first 5 seconds, when the air jet starts the cooling. The distribution shows also that the most important thermal gradients are situated in the YSZ layer, near the symmetry axis, where the center of the air jet impinges, while the temperature in the Inconel substrate is more homogeneous; the larger thermal conductivity of this layer in fact can dissipate efficiently the thermal gradients generated in the upper level. Simulations shows also that the sample is completely cooled within 300 s and reaches a homogeneous temperature of ~300 K.

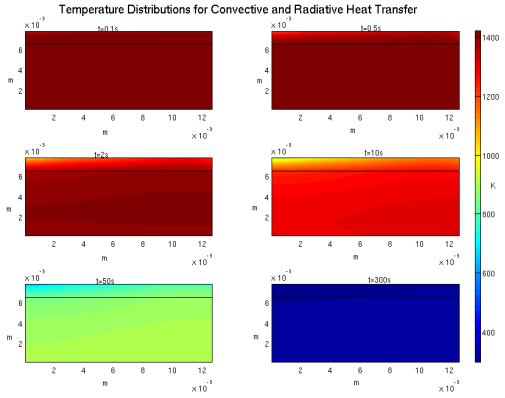

Fig 4. Temperature distribution vs time for convective and radiative heat transfer.

To better understand the influence of each contribution to the cooling, we also performed transient analysis for both only radiative cooling and only convective cooling on the same time scale. Results of the simulations are shown in Fig. 5 and 6. Fig. 5 shows that radiative heat transfer would provide a more homogeneous cooling of the sample. More over the simulations show that the only radiative cooling is a less efficient way than the convective one, even in the beginning of cooling where the contribution of the radiative heat transfer is higher as seen from (4). After 300 s the sample would reach the homogeneous temperature of ~800 K.

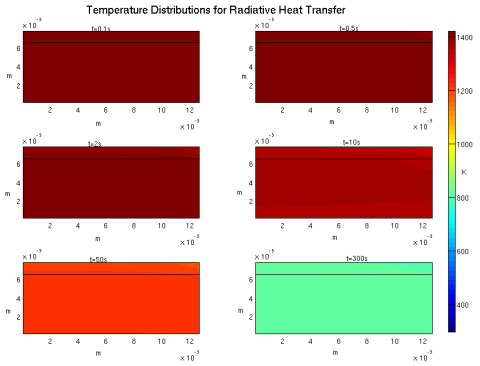

Fig 5. Temperature distribution vs time for radiative heat transfer.

The temperature distributions in Fig. 6 are obtained from a simulation that included only the presence of the jet and the natural convection as boundary conditions for the heat transfer. The distributions are similar to those obtained including also the radiative contributions to the heat transfer, confirming the hypothesis that the air jet represents the most important contribution to the cooling.

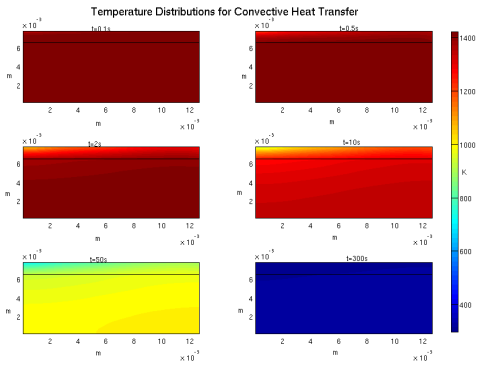

Fig 6. Temperature distribution vs time for convective heat transfer.

The thermal analysis results were included as thermal load in the mechanical stress coupled model.

Fig. 7 shows the shear stress distribution for different times; this kind of stress is responsible for the delamination processes of the coating [16]. As expected the biggest stresses are localized on the edge of the sample, at the interface between the YSZ and the Inconel layer. Simulations show also that this stress reaches its maximum values after about 200s, and then remain constant.

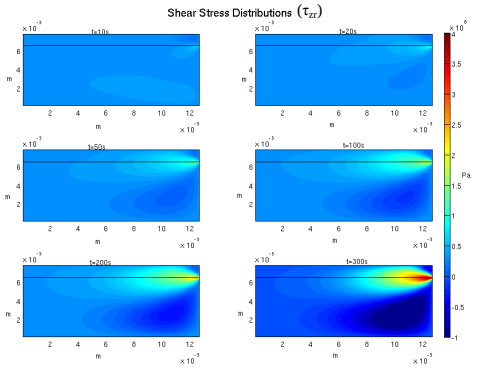

Fig 7. Shear stress distributions for different times in the r direction.

Fig. 8 shows the normal stress distribution obtained from the simulation. This kind of stress is responsible for the spallation processes of the coating [16]. As we expected the biggest stresses are localized on the YSZ-Inconel interface; in this case also the stresses reach their maximum values after about 200 s from the beginning of the cooling and then remain constant. For this kind of stress, the presence of the jet does provide an appreciable contribution within the first 10 seconds of the cooling on the Zirconia layer.

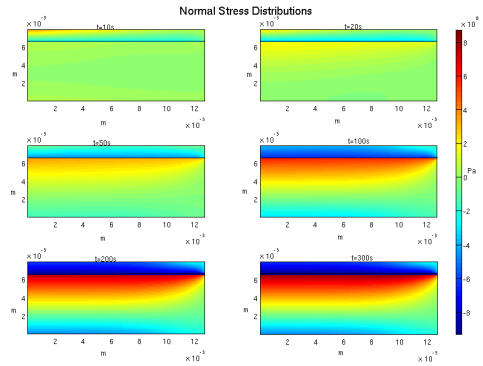

Fig 8. Normal stress distributions for different times in the z direction.

To validate the model we performed an experimental measuring of the sample temperature during the cooling under the impinging air jet. The sample was heated in the furnace until it reached the homogeneous temperature of ~1423 K and then it was pulled out and placed under the jet. The temperature was measured with a Raytek® Infrared Pyrometer model MM 2MH, with a spectral response of 1.6µm and a spot of 1mm; the pyrometer can work in the temperature range between 748 and 2498 K. We performed three experimental measurements to confirm our model. The data were collected in the point at the end of the transition region and the beginning of the wall jet region. The results are shown in Fig. 9; we included only the data after 5 seconds of cooling. Experimental data show good agreement with the simulated ones and validate our assumption that the MCrAlY layer could be included in the Inconel layer on the geometry.

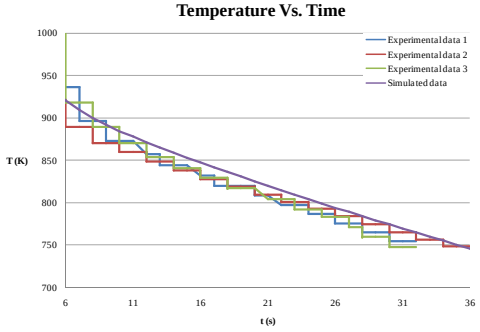

Fig. 9. Comparison between the simulated temperature and the experimental results.

5. Conclusions

In this paper we reported the assessment of a finite element model to predict the stress generation during the cooling of a TBC under an impinging air jet by COMSOL Multiphysics®. We performed a heat transfer analysis including both the radiative contribution and the convective one due to the present of the jet; the results were then included in the coupled structural mechanical stress-strain model as thermal load. Simulations show that the stresses are generated approximately on the first 200 seconds of cooling, and then they remain constant; moreover the results show that the sample is completely cooled in this condition after about 300 s of cooling. The thermal analysis' results show good agreement with the temperature measurements on real samples made by an optical pyrometer. This kind of study could be a useful tool to predict the sample behavior during the cooling and could help to design more efficient thermal cycling experiments.

6. References

[1] Huibin Xu, Shengkai Gong, Yue Zhang, Chunxia Zhang, Intermetallics 13, 315–322 (2005)

[2] Zhenghao Gan, Heong Wah Ng, Materials Science and Engineering A 385, 314–324 (2004)

[3] Michlik P., Berndt C., Surface & Coatings Technology 201, 2369–2380 (2006)

[4] D.R. Mumm, M. Watanabe, A.G. Evans, J.A. Pfaendtnerc, Acta Materialia 52, 1123–1131 (2004)

[5] Tilmann Beck, Roland Herzog, Olena Trunova, Marita Offermann, Rolf W. Steinbrech, Lorenz Singheiser, Surface & Coatings Technology 202, 5901–5908 (2008)

[6] Katti V., Prabhu S. V., International Journal of Heat and Mass Transfer 51, 4480–4495(2008)

[7] Miracle D. B., Acta Metallurgica et Materialia 41, 649 (1993)

[8] Saitoh M., Yoshiyasu I., Journal of Engineering for gas turbines and power 127, 807 (2005)

[9] Perry, R. H., Green, D. W. Perry's Chemical Engineers' Handbook 5-13, McGraw-Hill (7th edition 1997)

[10] Shackelford J. F, Alexander W., Materials Science and Engineering Handbook, Ed. James F. Shackelford & W. Alexander, Boca Raton: CRC Press LLC (2001)

[11] Tojo A., Atake T., Mori T., Yamamura H., J. Chem. Thermodynamics 31, 831–845 (1999)

[12] Pottlacher G., Hosaeus H., Kaschnitz E., Seifter A., Scandinavian Journal of Metallurgy 31, 161–168 (2002)

[13] Hayashi H., Saitoua T., Maruyama N., Inaba H., Kawamura, K., Mori M., Solid State Ionics 176, 613–619 (2005)

[14] Tang F., Schoenung J. M., Scripta Materialia 54, 1587–1592 (2006)

[15] Davis J. W., Iter Material Properties Handbook, pp. 1-6, Volume AD02-2111, Number 3 (1997)

[16] Bhatnagar H., Ghosh S., Walter M. E., International Journal of Solids and Structures 43, 4384–4406 (2006)